Supplement of The Cryosphere, 19, 3971–3989, 2025
https://doi.org/10.5194/tc-19-3971-2025-supplement

The Cryosphere Open Access EGU

Supplement of

Short and Long-term Grounding Zone Dynamics of Amery Ice Shelf, East Antarctica

Yikai Zhu et al.

Correspondence to: Yikai Zhu (y.zhu3@leeds.ac.uk)

Supplementary

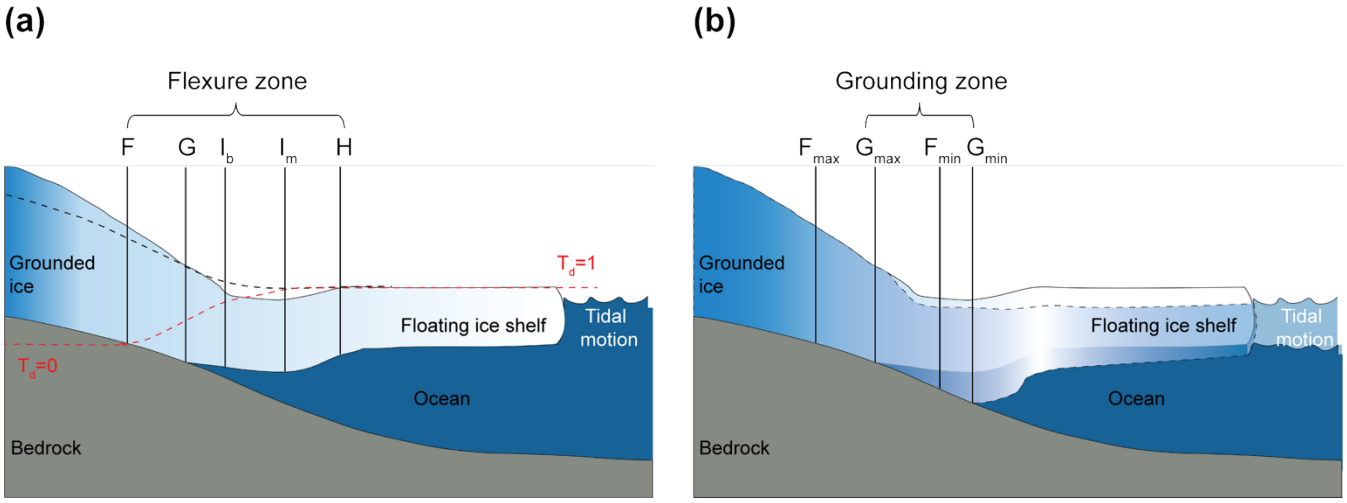

Figure S1. (a) Idealized Schematic of an ice plain flexure zone (FZ): This diagram illustrates an ice plain FZ while neglecting potential short-term and long-term GL migration. It highlights key satellite-derived GL proxies, including: Point G is the true GL where the grounded ice first loses contact with the bed; Point F is the landward limit of ice flexure driven by tidal motion; Point I_b is the break in slope; Point I_m is the local minimum in topography; and Point H is the seaward limit of ice flexure and the landward limit of stable hydrostatic equilibrium. The black dashed line is the hydrostatic ice surface (i.e. the hypothetic elevation of the ice in hydrostatic equilibrium). **(b)** Idealized Schematic of an ice plain grounding zone (GZ): This diagram illustrates the tidal short-term GL migration, highlighting the differences in the position of the ice shelf and the migration of Points F and G between high tide (F_{max}, G_{max}) and low tide (F_{min}, G_{min}). This illustration accounts for the influence of tidal motion on GL position, showing the dynamic nature of the GZ over tidal cycles (adapted from Brunt et al., 2010, 2011 and Friedl et al., 2019).

Table S1. List of Sentinel-1 SAR image acquisition dates used for each DROT measurement.

Index	Dates (dd/mm/yyyy)
D1	31/01/2021-06/02/2021-12/02/2021
D2	06/02/2021-12/02/2021-18/02/2021
D3	12/02/2021-10/02/2021-24/02/2021
D4	24/02/2021-02/03/2021-08/02/2021
D5	02/03/2021-08/03/2021-14/03/2021
D6	08/03/2021-14/03/2021-20/03/2021

D7	14/03/2021-20/03/2021-26/03/2021
D8	20/03/2021-26/03/2021-01/04/2021
D9	26/03/2021-01/04/2021-07/04/2021
D10	07/04/2021-13/04/2021-19/04/2021
D11	13/04/2021-19/04/2021-25/04/2021
D12	19/05/2021-25/05/2021-31/05/2021
D13	31/05/2021-06/06/2021-17/06/2021
D14	06/06/2021-12/06/2021-18/062021
D15	12/06/2021-18/06/2021-24/08/2021
D16	18/06/2021-24/06/2021-30/06/2021
D17	06/07/2021-12/07/2021-18/07/2021
D18	12/07/2021-18/07/2021-24/07/2021
D19	05/08/2021-11/08/2021-17/08/2021
D20	11/08/2021-17/08/2021-23/08/2021
D21	17/08//2021-23/08/2021-29/08/2021
D22	23/08/2021-29/08/2021-04/09/2021
D23	29/08/2021-04/09/2021-10/09/2021
D24	04/09/2021-10/09/2021-16/09/2021
D25	10/09/2021-16/09/2021-22/09/2021
D26	22/09/2021-28/09/-2021-04/10/2021
D27	28/09/2021-04/10/2021-10/10/2021
D28	04/10/2021-10/10/2021-16/10/2021
D29	10/10/2021-16/10/2021-22/10/2021
D30	28/10/2021-03/11/2021-09/11/2021
D31	09/11/2021-15/11/2021-21/11/2021
D32	15/11/2021-21/11/2021-27/11/2021

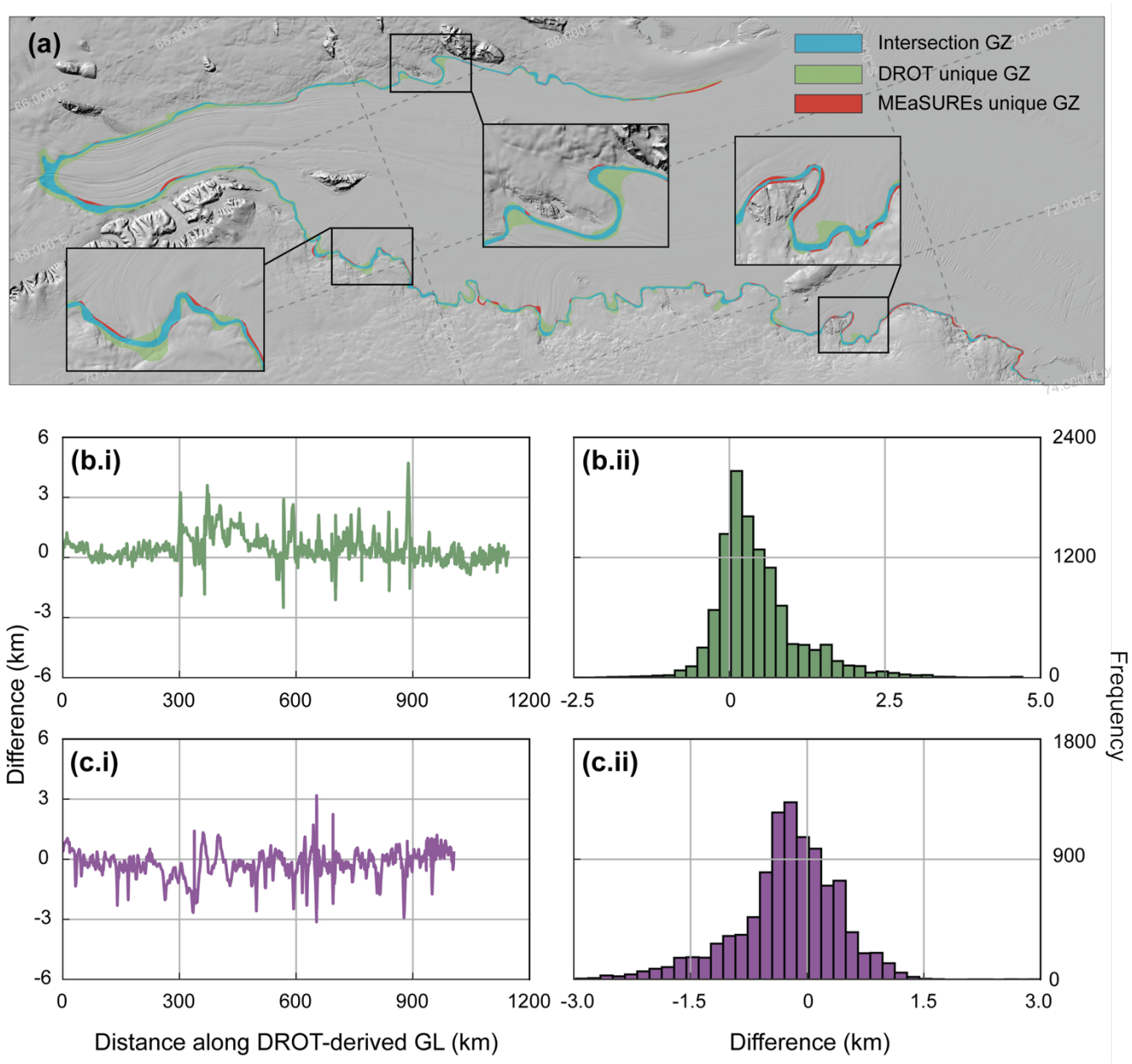

Figure S2. Comparison of DROT-derived GZ and MEaSUREs Antarctic GZ Version1 (MAGZv1) dataset (Rignot et al., 2023). **(a)** Overview map showing the spatial agreement and discrepancy between the two results. The blue segments represent the intersection area between the two GZs, while green and red segments represent regions uniquely identified by the DROT-derived GZ and MAGZv1, respectively. Insets highlight representative regions where the differences are more pronounced for visual clarity. **(b.i-c.i)** Along-track comparison of the landward (green) and seaward (purple) GZ boundaries between the DROT-derived GZ and MAGZv1, with distance computed along the DROT-derived GZ boundary. **(b.ii-c.ii)** Histograms showing the distribution of differences between the DROT-derived and MAGZv1 boundaries for landward (green) and seaward (purple) edges, respectively.

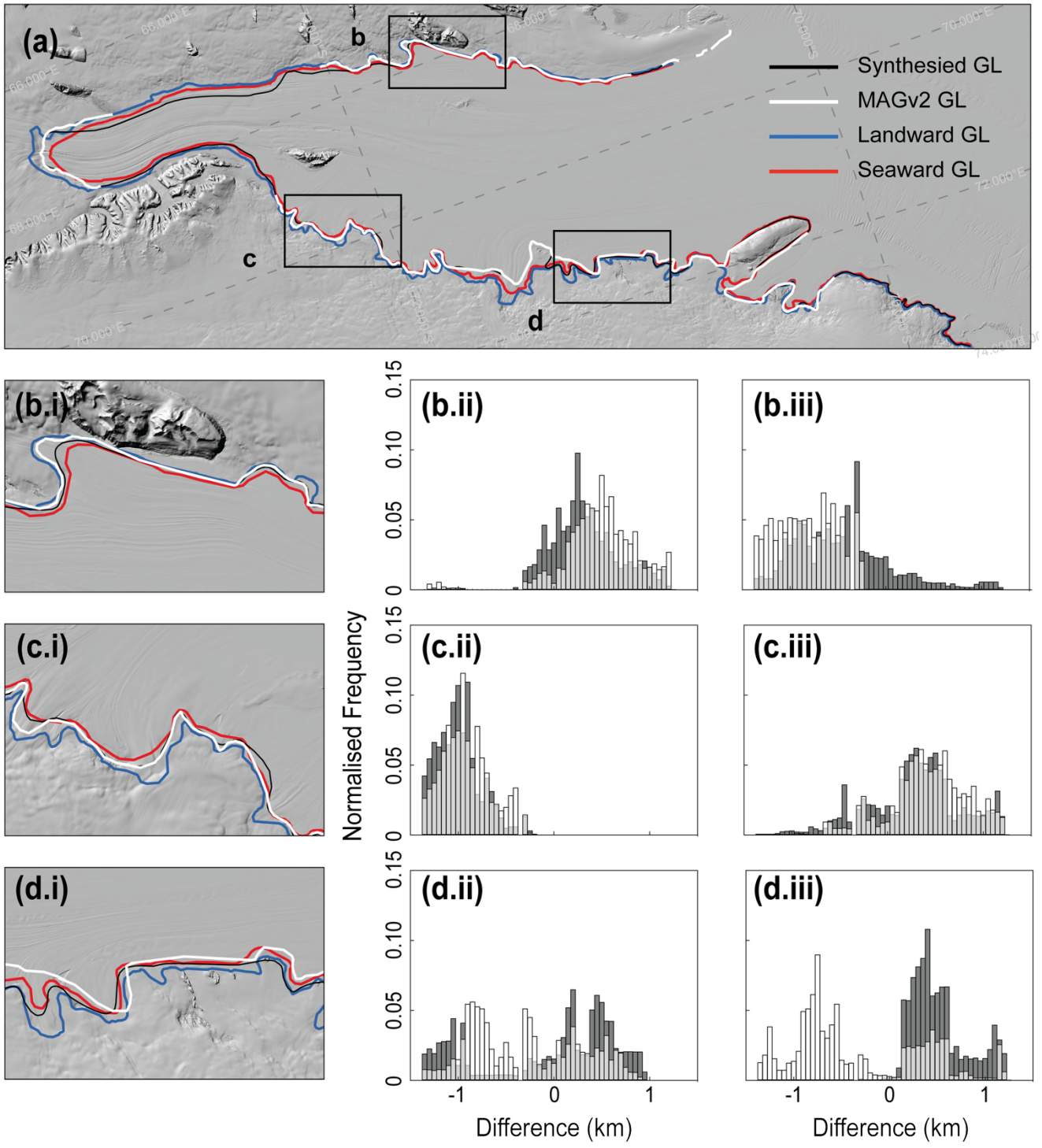

35 **Figure S3.** Comparison of DROT-derived GLs and two published GL datasets. **(a)** Overview map showing the comparison between the DROT-derived landward (blue) and seaward (red) GLs with two published GL datasets: MAGLv2 (white) and Synthesized GL (black). **(b.i-**

d.i) Zoomed in maps of the three selected locations labelled b to d from panel **(a)**, showing the spatial differences between the DROT-derived GLs and the published GL datasets. **(b.ii-d.ii)** Histograms show the distribution of difference between the DROT-derived landward GL and two published GL datasets along the GL in all three sub-regions. **(b.iii-d.iii)** Histograms show the distribution of difference between the DROT-derived seaward GL and the two published GL datasets along the GL in all three sub-regions. The white bars represent the difference between the DROT-derived GL and the MAGv2, while the grey bars represent the difference between the DROT-derived GL and the Synthesized GL.

Table S2. Mean absolute separation and standard deviation between the DROT-derived GL and other comparable GL datasets for the AmIS region, including the MAGv2 (Rignot et al., 2016), and the Synthesized GL (Depoorter et al., 2013). The terms "landward GL" and "seaward GL" refer to the GLs closest to the ocean and closest to the land, respectively, among the 32 DROT-derived GLs. Positive values indicate that the DROT-derived GL is located closer to the ocean compared to the two published datasets.

GL datasets	Landward GL		Seaward GL	
	Mean absolute separation (km)	Standard deviation (km)	Mean absolute separation (km)	Standard deviation (km)
DROT vs MAGv2	1.59	2.16	1.45	1.79
DROT vs Synthesized GL	1.55	2.11	1.27	1.74
MAGv2 vs Synthesized GL	0.68	0.86	0.68	0.86

*Note: MAGv2 vs Synthesized GL values represent overall differences, not split by Landward/Seaward.

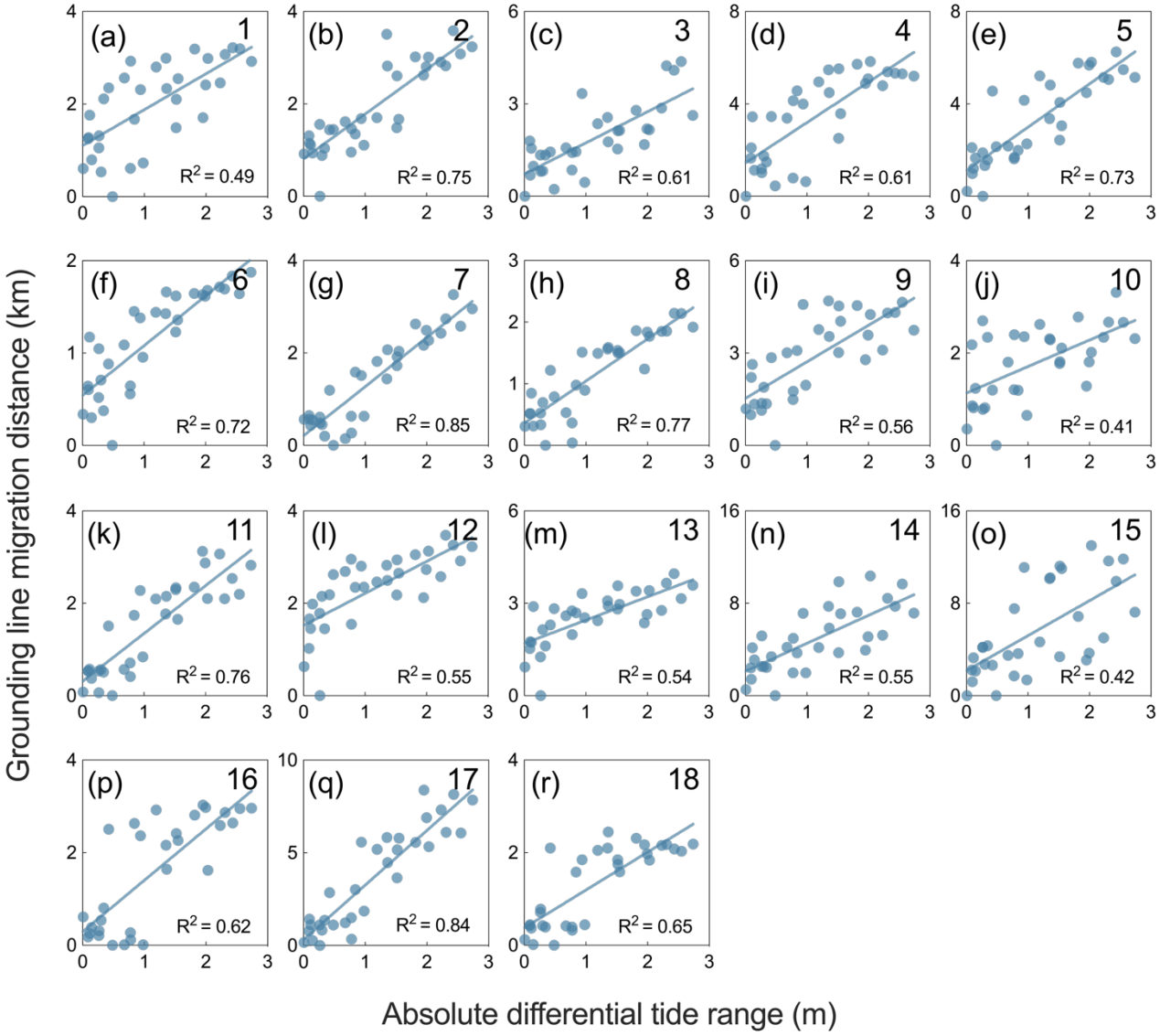

Figure S4. GL migration distance versus absolute differential tide range across various profiles. The label in the upper right corner of each subplot indicates the corresponding profile number, consistent with the profile numbering in Figure 1b. The solid blue lines indicate the linear fitting results, showing the relationship between GL migration distance and absolute differential tide range. Note that a GL migration distance of 0 km represents the location of the seawardmost GL observed in each profile, which is used as the reference point for calculating relative migration distances.

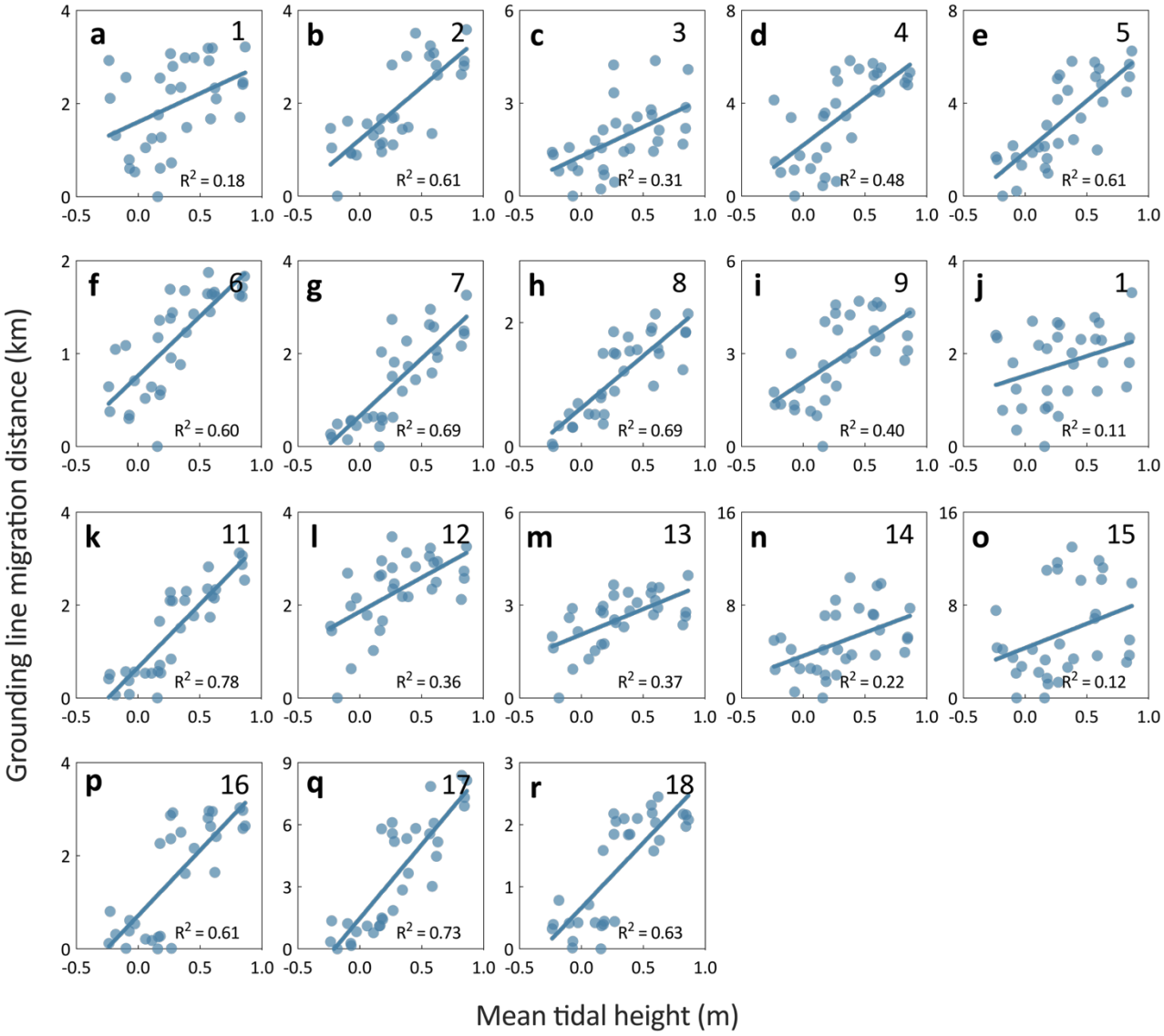

Figure S5. GL migration distance versus mean tide height across various profiles. The label in the upper right corner of each subplot indicates the corresponding profile number, consistent with the profile numbering in Figure 1b. The solid blue lines indicate the linear fitting results, showing the relationship between GL migration distance and mean tide height. Note that a GL migration distance of 0 km represents the location of the seawardmost GL observed in each profile, which is used as the reference point for calculating relative migration distances.

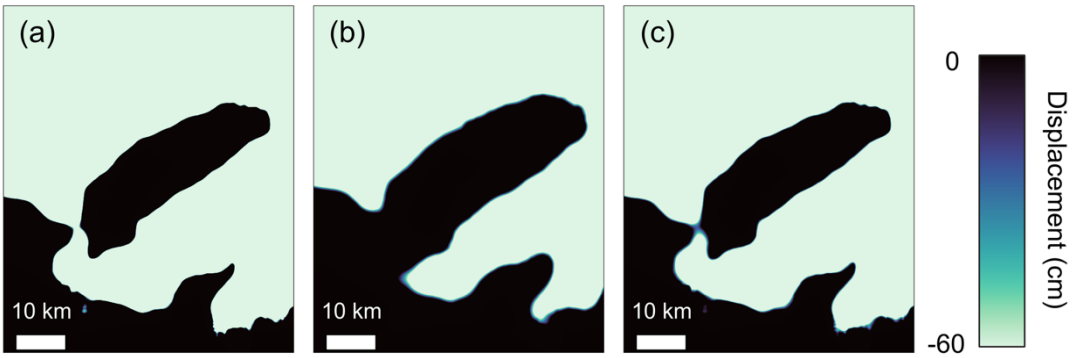

Figure S6. DROT results showing different grounding states between the Gillock Island and the ice sheet across three time periods: **(a)** grounded state from 31/01/2021–06/02/2021–12/02/2021; **(b)** ungrounded state from 19/05/2021–25/05/2021–31/05/2021; **(c)** grounded state from 12/06/2021–18/06/2021–24/06/2021. The colour scale corresponds to the amount of tidally induced vertical displacement.

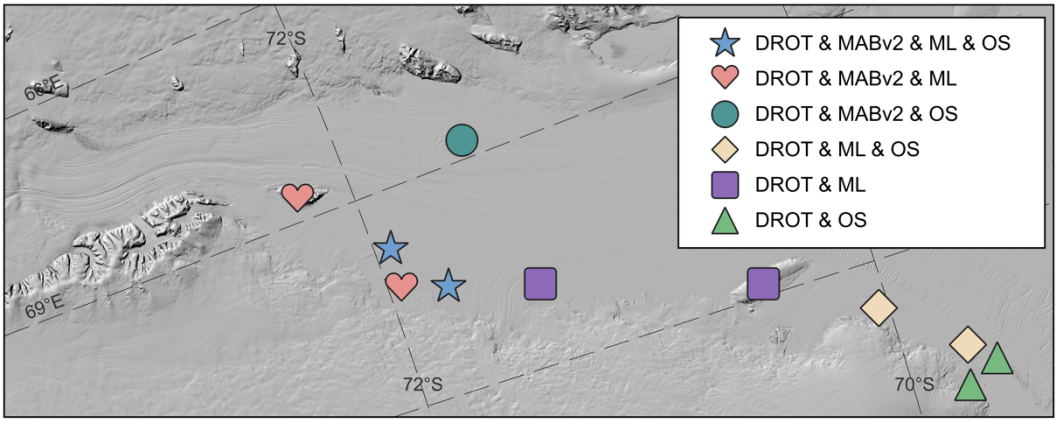

Figure S7. Pinning points measured using DROT, MEaSUREs Antarctic Boundaries v2 (MABv2) data (Rignot et al., 2016), machine learning (ML) (Mohajerani et al., 2021), and optical shadow (OS) data (Miles and Bingham, 2024). Pinning points are classified according to whether they appear in: DROT, MABv2 data, ML, and OS (pink star); only DROT, MABv2 data and ML (pink heart); only DROT, MABv2 data, and OS (teal circle); only DROT, ML, and OS (yellow diamond); only DROT and ML (purple rectangle) and only DROT and OS (green triangle).

Reference

Depoorter, M. A., Bamber, J. L., Griggs, J., Lenaerts, J. T. M., Ligtenberg, S. R. M., Broeke, M. R. van den, and Moholdt, G.: Synthesized grounding line and ice shelf mask for Antarctica, , https://doi.org/10.1594/PANGAEA.819151, 2013.

Miles, B. W. and Bingham, R. G.: Progressive unanchoring of Antarctic ice shelves since 1973, Nature, 626, 785–791, https://doi.org/10.1038/s41586-024-07049-0, 2024.

Mohajerani, Y., Jeong, S., Scheuchl, B., Velicogna, I., Rignot, E., and Milillo, P.: Automatic delineation of glacier grounding lines in differential interferometric synthetic-aperture radar data using deep learning, Scientific reports, 11, 4992, https://doi.org/10.1038/s41598-021-84309-3, 2021.

Rignot, E., Mouginot, J., and Scheuchl, B.: MEaSUREs Antarctic Grounding Line from Differential Satellite Radar Interferometry, Version 2, https://doi.org/10.5067/IKBWW4RYHF1Q, 2016.

Rignot, E., Mouginot, J., and Scheuchl, B.: MEaSUREs Grounding Zone of the Antarctic Ice Sheet, Version 1, , https://doi.org/10.5067/HGLT8XB480E4, 2023.